Theoretical studies of interactions of atoms, molecules, and surfaces:

Particle–surface and laser–atom interactions

Uwe Thumm, J.R. Macdonald Laboratory, Kansas State University, Manhattan, KS 66506
thumm@phys.ksu.edu

1. Electron capture from thin metallic films

Recent progress: Based on the self-energy method [1,2] for charge transfer in ion–surface collision, we are investigating the broadening of atomic levels near thin metallic films. Size quantization in the growth direction of the film gives rise to characteristic structures in level widths, atomic occupation probabilities, and transition distances as a function of the film thickness [3]. Details of this structure depend on the orientation of the atomic Stark orbitals with respect to the film and can be related to the dependence of transition matrix elements on the active electron's wave vector component parallel to the surface. The large variation of the calculated transition distances with the film thickness may result in observable effects in atomic interactions with thin films.

Future plans: We plan to calculate the full electronic self-energy of hydrogenic atoms interacting with thin metallic films. Adiabatic resonance states generated from the self-energy for thin film targets will serve as basis states in time-dependent close-coupling calculations for the electronic dynamics in atom-film interactions, in close analogy to the semi-infinite case of a metal surface [4,5,6]. The extension of the present calculations to the case of layered nano–structures composed of arbitrary sequences of metals, semiconductors, and insulators, and involving arbitrary z-profiles, is straightforward. Possible applications of calculations of this kind may be found, e.g., in the analysis of electron transfer in ion desorption processes. These processes have considerable practical relevance in surface and thin film analytical methods.

2. Charge–transfer dynamics near metal surfaces

Recent progress: Within a new two-center close-coupling expansion, we solved the time-dependent Schrödinger equation for an active electron interacting with a slow projectile and a metal surface. The continuum of metal conduction band states is discretized in terms of wave packets. We obtained converged results for the time evolution of the atomic and metallic population amplitudes for an excited hydrogen atom near an aluminum surface [5,7,8]. In contrast to the self–energy approach [1], the continuum discretization resolves the active election's motion in the metal Hilbert space and allows for the study of projectile energy loss due to electron–hole pair excitations in the substrate.

Future plans: The efficient discretization of (ionization or conduction band) continua is an outstanding problem that requires the (often neglected) careful analysis of convergence, dephasing, and recurrence effects [6]. We intend to streamline our code and to increase the number of states that represent the discretized conduction band continuum in order to fully eliminate recurrence effects, even at very slow projectile velocities. We also intend to investigate the projectile energy loss due to electron–hole pair and plasmon excitations in the substrate.

3. Wave-packet propagation techniques applied to ion-surface interactions

Recent progress: Apart from contributing to the qualitative understanding of the interaction mechanisms, e.g., through computer animations, the direct propagation of the wave function on a numerical grid also enables the quantitative assessment of (one–electron) charge transfer. This method is flexible in that there are practically no restrictions on the effective one–electron potential used to describe the surface and projectile electronic structure (and the perturbations induced during the interaction).

Resonance positions and widths can be obtained by propagating the initial electronic state of the projectile Ψ_0 under the influence of the surface potential while keeping the ion at a *fixed* location $\vec{D}$ in front of the surface. The wave function at any time t is given by (unless stated otherwise, we use atomic units)

$$\Psi(\vec{r},\vec{D},t) = \exp\{-iH(\vec{r},\vec{D})\,t\}\ \Psi_0(\vec{r},\vec{D})\ , \quad H = T + V_{surface} + V_{atom} \tag{1}$$

The ion–survival probability is obtained by following the reflected projectile until the integrated probability density around the projectile has reached a stable value.

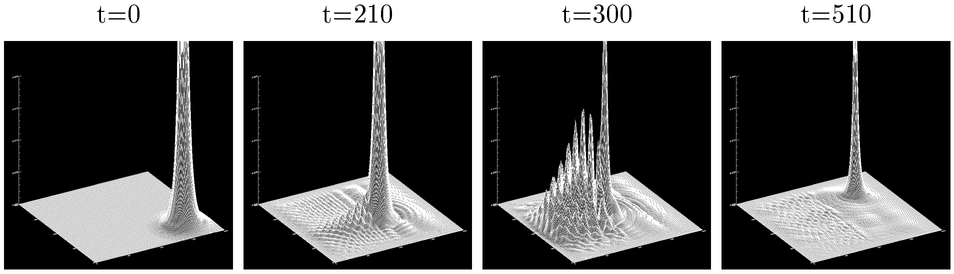

Fig. 1. Charge–transfer during the interaction of H^- ions with a model aluminum surface.

Fig. 1 shows the electronic probability density evolution for the scattering of H^- on a metal surface. The ion comes from the lower right corner of the x–z plane and is reflected to the upper left corner. The plot shows $ln|\psi(x,0,z,t)|^2$ obtained by three dimensional wave function propagation. The exploratory calculation is based on the corrugated surface potential

$$V_{surface}(\vec{r}) = 0.5[\Theta(z) - 1][1 + 0.5\cos(x)\cos(y)\cos(z)], \qquad \Theta(z) = atan(z)/\pi + 0.5. \tag{2}$$

Θ is a smeared–out step function. The effective potential for H^- was modeled by regularizing

$$V_{atom}(r_p) = -(1 + \frac{1}{r_p})\exp(-2r_p) - \frac{\alpha}{r_p^4}\exp(-\frac{r_0^2}{r_p^2}) \tag{3}$$

at the origin. r_p measures the distance from the projectile center, $\alpha = 2.25$ is the atomic polarizability of H, and $r_0^2 = 2.547$. V_{atom} allows for the computation of the negative–ion ground state Ψ_0 of H^- and reproduces its affinity (0.75 eV). The propagator in (1) was constructed using the split–operator Crank–Nicholson technique on a 251 x 151 x 251 numerical grid with constant grid spacing, covering 100 x 60 x 100. a.u.^{3} in coordinate space. The projectile was led along a broken–straight–line trajectory, starting at $t = 0$ at a distance of 30 a.u. from the jellium edge of the surface with an incident velocity $(v_x, v_z) = (0.1, -0.1)$ and with $d_{min} = 2$. Boundary conditions at the edge of the grid were imposed by a suitable absorptive complex potential. Shortly after $t = 510$ (last frame in Fig. 1), the resonant flux of electron probability density has stopped. The ion–survival probability, obtained by integration over the atomic probability density at $t = 600$ amounts to 0.07.

Future plans: We intend a detailed investigation of the influence of crystal orientation, surface states, and image states of the substrate on the transfer of charge to and from a projectile.

4. Ionization in intense laser fields: distribution of emitted electron momenta

Recent progress: The basic features of single ionization by a strong, short laser pulse can be studied within the restricted dimensionality of a 1D model atom. Such a model target is given by the soft-core Coulomb potential, $V_{1D}(x) = -\frac{\gamma}{\sqrt{x^2+\alpha^2}}$, with parameters $\alpha = \gamma = 1$. The ground state $\psi_0(x)$ in this potential is bound with $\epsilon_i = 18.23\ eV$.

We expose this atom to a laser pulse of the form $V_L(x,t) = E_0 f(t) sin(\omega t)x$, with a Gaussian envelope function f(t) of width (FWHM) of 500. We further assume a laser wavelength of 780 nm, corresponding to the angular frequency $\omega = 0.0584$ and period $T = 107.59$. An assumed intensity of $I = 10^{15}\ W/cm^2 = 0.0285$ corresponds to an electric field amplitude $E_0 = 8.69 \times 10^8\ V/cm = 0.169$.

The given values of laser frequency, intensity and atom binding energy result in a ponderomotive energy of $U_p = I/(4\omega^2) = 57.6\ eV = 2.1$, a maximal classical excursion range of the electron of $x_{exc} = 4.46\ E_0/\omega^2 = 221$, and a Keldysh parameter $\gamma = \sqrt{\epsilon_i/(2U_p)} = 0.4$. The value of $\gamma < 1$ tends to favor tunneling as the most likely ionization mechanism.

Due to the interaction of the atom with the laser pulse, the electronic wave function evolves according to

$$\psi(x,t) = \exp\{-i\int^t dt' H(x,t')\}\,\psi_0(x) \tag{4}$$

where the Hamiltonian is given by $H(x,t) = T + V_{1D}(x) + V_L(x,t)$, with T for the electron's kinetic energy.

We obtain the time-dependent wave function $\psi(x,t)$ by numerically propagating ψ_0 using the split-operator, Cranck-Nicholson method. We use time increments $\delta t = 0.03$ and equally spaced spatial grid points that are $\delta x = 0.23$ apart. The spatial grid extents from $x_{min} = -280$ to $x_{max} = 280$ with the atom located at the center ($x = 0$). The stability parameter $\delta t/(2\delta x^2) = 0.31$ is smaller than one, as required for numerical stability. At the edges of the spatial grid, that is for $|x| > 250$, we introduce an absorptive potential in order to avoid non–physical reflections of probability density and in order to impose the correct boundary condition for ionization.

Recent photoionization experiments have determined the emitted electron momentum distribution for single ionization. In order to extract momentum-differential emission probabilities from our calculation, we introduce small 'detection intervals' to the right and to the left of the atom that lie outside the classical excursion range x_{exc} of the electron. We choose these intervals at $I_L = [-250, -225]$ and $I_R = [225, 250]$. Next, we define a momentum grid $\{p_j\}$ with step size $\delta p = 0.04$. δp is slightly smaller than a typical momentum resolution in recoil momentum experiments of $\delta p_{exp} = 0.1$. The largest momentum that we can represent on our spatial grid is given by Nyquist's formula as $1/(2\delta x) = 2.2$.

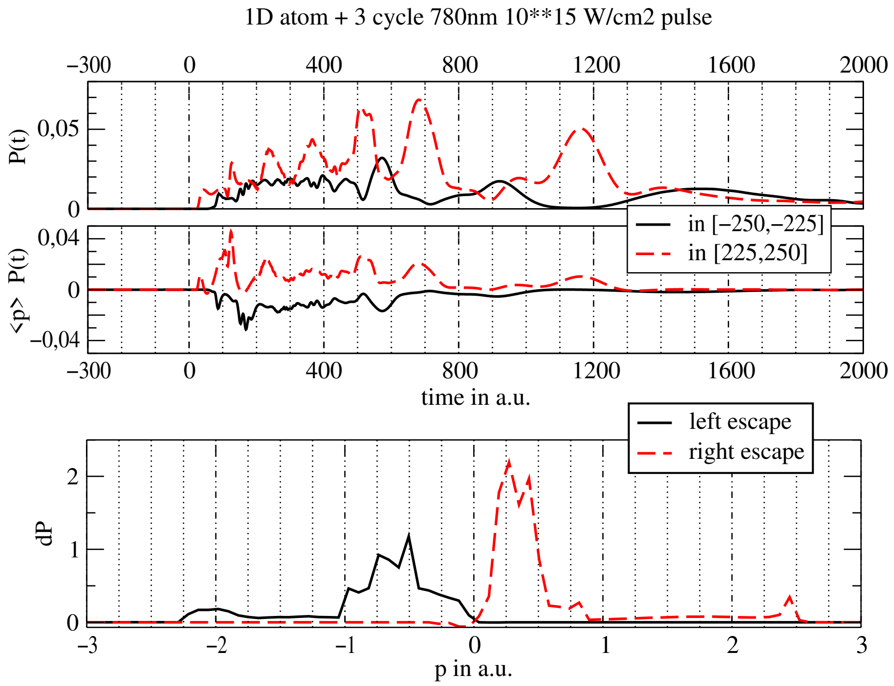

Fig. 2. Probability for finding the emitted electron at distances from the nucleus between [-250,-225] and [225,250] (top). Electronic current through these intervals (middle). Momentum distribution of emitted electrons (bottom).

The probability $dP_R(p_j, \delta p)$ for emission of an electron with momenta in the interval $I(p_j, \delta p) = [p_j - \delta p/2, p_j + \delta p/2]$ can now be related to the 1D released current

$$j_R = Re\{\int_{I_R} dx\ \psi^* p \psi\} \approx -\frac{1}{2} Re\{i \sum_{x_j \in I_R} \psi(x_j)^* (\psi(x_{j+1}) - \psi(x_{j-1}))\} \tag{5}$$

according to

$$dP_R(p_j, \delta p) = \int dt\ j_R \begin{cases} 1 & if < p >_R \in I(p_j, \delta p) \\ 0 & else \end{cases} \tag{6}$$

where $< p >_R$ is the momentum expectation value in the interval I_R. For emission to the left, $j_L, dP_L, < p >_L$ are obtained in the same way.

The top graph in Fig. 2 shows the probability for finding the electron in I_R and I_L for a three cycle pulse. Clearly visible are jets that arrive in the right interval I_R at multiples of the laser period. The middle graph shows j_R and j_L as functions of time. The fastest emitted electrons reach the detection interval I_R at $t \approx 50$; the slowest at $t \approx 1200$, long after the laser pulse. The momentum distributions dP_R and dP_L in the lowest graph indicate most likely emission of electrons with momenta between 0.15 and 0.5 to the right and between -0.9 and -0.2 to the left. The addition of dP_R and dP_L shows a dip around momenta $p = 0$, in qualitative agreement with the double-hump momentum distribution found in recent single ionization measurements.

Future plans: We intend to investigate the Fourier transform of $C(t) = \int dx\ \psi(x,t)^* \psi_0(x)$ in an attempt to identify and characterize field–induced resonances. We have started to investigate double ionization of 2D model atoms.

References

[1] "Resonance formation of hydrogenic levels in front of metal surfaces," P. Kürpick, U. Thumm, U. Wille, Phys. Rev. A 56, 543 (1997).

[2] "Hybridization of ionic levels at metal surfaces," P. Kürpick, U. Thumm, Phys. Rev. A 58, 2174 (1998).

[3] "Size quantization effects in atomic level broadening near thin metallic films," U. Thumm, P. Kuerpick, U. Wille, Phys. Rev. B 61, 3067 (2000).

[4] "Ionization of atoms interacting with a metal surface under the influence of an external electric field," P. Kürpick, U. Thumm, U. Wille, Phys. Rev. A 57, 1920 (1998).

[5] "Electron dynamics and level broadening in slow atomic interactions with metal surfaces and thin metallic films" B. Bahrim, P. Kürpick, U. Thumm, U. Wille, Nucl. Instr. and Meth. B 164, 614 (2000).

[6] "Charge transfer and electron emission in ion–surface collisions," U. Thumm, J. Ducrée, P. Kürpick, U. Wille, Nucl. Inst. Meth. B 157, 11 (1999).

[7] " Electron transfer and orbital hybridization in slow collisions between excited hydrogen atoms and aluminum surfaces", B. Bahrim and U. Thumm, submitted to Phys. Rev. A

[8] "Ion–Surface Interactions", U. Thumm, ICPEAC 2001 invited paper, to appear.

Other publications of DOE sponsored research during 1998 – 2000

• "The low–lying negative–ion states of Rb, Cs, and Fr," C. Bahrim and U. Thumm, Phys. Rev. A 61, 022722 (2000).

• "Charge–transfer dynamics in slow atom-surface collisions: a new close-coupling approach including continuum discretization," B. Bahrim and U. Thumm, Surface Science 451, 1 (2000).

• "Neutralization of hyperthermal multiply charged ions at surfaces: comparison between the extended dynamical over–barrier model and experiment," J. Ducrée, H.J. Andrä, U. Thumm, Phys. Rev. A 60, 3029 (1999).

• "Improved simuation of highly charged ion–surface collisions," Ducrée, H.J. Andrä, U. Thumm, Physica Scripta T 80, 220 (1999).

• "Angular differential cross sections in slow ion–C_{60} interactions," L. Hägg, A. Barany, H. Cederquist, U. Thumm, Physica Scripta T 80, 205 (1999).

• "Soft collisions of highly charged ions with C_{60}," U. Thumm, Comments At. Mol. Phys. 34, 119 (1999).

• "Extended classical over-barrier model for collisions of highly charged ions with conducting and insulating ionic crystals surfaces," J.J. Ducrée, F. Casali, U. Thumm, Phys. Rev. A 57, 338 (1998).

• "Angular distributions of projectiles following electron capture from C_{60} by 2.5 keV Ar^{8+}, " B. Walch, U. Thumm, M.Stöckli, C. L. Cocke, Phys. Rev. A 58, 1261 (1998).